Feedback linearization based sensorless direct torque control using stator flux MRAS-sliding mode observer for induction motor drive

Abdelkarim Ammar, Aissa Kheldoun, Brahim Metidji, Tarek Ameid, Younes Azzoug

Feedback linearization based sensorless Direct Torque Control using stator flux MRAS-sliding mode observer for induction motor drive

Abdelkarim AMMAR[1 2*] Aissa KHELDOUN[1], Brahim METIDJI[1], Tarek AMIED[3], Younes AZZOUG[2 3]
[1]Signals and Systems Laboratory (LSS), Institute of Electrical and Electronic Engineering, University of M'hamed BOUGARA of Boumerdes, Boumerdes, Algeria.
[2] Electrical Engineering Laboratory of Biskra (LGEB), Electrical Engineering Department, University of Mohamed KHIDER of Biskra, Algeria
[3] Faculty of Applied Science, Univ. Artois, EA 4025 LSEE F-62400, Béthune, France

Abstract

The high-performance Direct Torque Control (DTC) requires accurate knowledge of flux and speed information. Furthermore, the elimination of sensors leads to reduced overall cost and size of the electric drive system and subsequently improving its reliability. This paper proposes an effective sensorless direct torque control scheme for induction motor drive. The proposed scheme consists of enhancing the decoupling structure and variable estimation as well. Therefore, an enhanced direct flux and torque control based on feedback linearization is implemented in one hand. This allows obtaining a linear decoupled control together with minimized flux and torque ripples. In another hand, a combined sliding mode observer and model reference adaptive system is associated with the control scheme as sensorless algorithms for rotor speed and flux estimation. This conjunction is intended to enhance the sliding mode observer performances especially at low speed operations and reduce its sensitivity to noise and system uncertainties as well. The effectiveness of the proposed control algorithm has been verified through simulation and experimental work using MATLAB/Simulink software and dSpace 1104 implementation board respectively.

Keyword

Induction motor, Direct Torque Control, Feedback Linearization, Sliding Mode Observer, Model Reference Adaptive System, Sensorless control.

1. Introduction

The Direct Torque Control (DTC) offers many advantages, such as simplicity, fast response and less sensitivity to machine parameters when it is compared to the field oriented control (FOC) [1]. The integration of the space vector modulation (SVM) instead of the switching table in the DTC control scheme was a very helpful solution [2]. SVM based-DTC offers fixed switching frequency, higher DC voltage utilization ratio and lower harmonics distortion [3]. Therefore, it provides reduced ripples and lower switching losses, unlike conventional DTC. However, SVM-DTC relies on linear proportional-integral (PI) controllers and the field-oriented reference frame [4]. The latter requests coordinates transformation which increases the complexity of the control's algorithm. Besides, the linear controllers can be not sufficient to deal with a high degree of uncertainty like the nonlinear coupling of the machine, external disturbances or parameters variation [5,6]. In order to address these problems and improve the motor control ability and variables decoupling, several control theories have been arisen, in which the robust nonlinear control techniques are widely mentioned in automatic and electrical drives field. Among these, the input-output feedback linearization (IOFL) is a popular method [7,8]. The feedback linearization is a model-based approach which can disappear the coupling effect and improve the control performance. It converts the nonlinear system into an equivalent linear to become simpler for control design [9,10]. IOFL has been suggested to improve SVM-DTC in several works [11,12]. It can guarantee a good decoupling of the motor torque

and stator flux. In addition, it reduces the design complexity by avoiding the coordinate transformation. Thus, this control method gives a possibility to get better behavior in both dynamic and steady states [13].

However, the application of advanced control strategies needs an accurate speed and flux measurement or estimation for closed-loop control design. The measurement process is associated with several difficulties especially the high cost and the fragility of the sensors. Besides, the physical environment sometimes does not tolerate to use sensors [14]. Hence, eliminating them to reduce the cost and the volume of the drive system and to increase its reliability is of utmost importance. Various model-based approaches have been proposed in the literature for sensorless control of AC electrical drives [15]. Which can estimate the motor speed in closed loop using only the instantaneous measurement of voltages and currents. Full order observers and Kalman filters [16,17] are amongst these approaches. Moreover, the sliding mode theory has proven its effectiveness in estimation as well as in the controllers design [18,19]. It can be selected due to its many advantages such as ease of implementation, high robustness and low computation requirements [20].

To this, diverse structures of sliding mode observers (SMOs) have been proposed during the last decade for speed and flux estimation [21,22]. In general, sensorless algorithms in motor drives work well in the medium and high-speed ranges but lacks accuracy and robustness at very low speeds particularly around zero excitation frequency. In fact, in the low-speed range, the drive becomes unstable and the torque capability decreases which cause an inaccurate speed regulation. Some developed SMOs designs do not employ the speed adaptation scheme have been proposed in [23,24]. This means that they do not take the speed as an adaptive quantity. In these observers, the speed estimator is completely separated from the main flux observer in order to increase the accuracy at low rotor speed and to reduce observer complexity [20]. Usually, these types of observers use an open-loop estimator based on flux derivation to reconstruct the rotor speed. This derivation may be sensitive to noise which needs to be filtered out. However, the overuse of filters introduces a delay in the signal acquisition and this may lead to undesirable effects. In this work, a model reference adaptive system (MRAS) estimator is associated with the sliding mode observer to carry out the speed estimation. Where, the stator flux sliding mode observer will takes the place of the reference voltage model of MRAS. The stator-flux based MRAS is adopted to be more suitable for DTC control design and to reduce observer complexity [25].

The main goal of this paper is to design an improved sensorless direct flux and torque control for induction motor drives. The algorithm is composed of a feedback linearization controller that is associated with MRAS-sliding mode observer for flux and speed estimation. The performance of the proposed control and estimation strategies are investigated through simulation using MATLAB/Simulink software and validated through experimental implementation using dSpace 1104 real-time interface (RTI).

This paper is organized as follows: Section 2 presents the induction machine mathematical model while section 3 is devoted to the design of the direct torque control via the feedback linearization and the space vector modulation. The design of sliding mode

flux observer with the open loop speed estimator is given in Section 4. After that, Section 5 presents the association of the model reference adaptive system with SMO. Simulation results of the proposed control and estimation techniques together with their discussions are given in section 6. Section 7 presents the results of the experimental validation and finally, the paper ends up with a general conclusion.

Nomenclature

DTC	*Direct Torque Control.*	ψ_s	Stator flux vector.
SVM	*Space Vector Modulation.*	p	Number of pole pairs.
IOFL	*Input-Output Feedback Linearization.*	V_1 V_2	Auxiliary inputs of the control technique.
SMC	*Sliding Mode Control.*	k_1 k_2	Positive constants of the control technique.
SMO	*Sliding Mode Observer.*	T_z	Sampling time.
$i_{s\alpha}$ $i_{s\beta}$	*α and β components of stator currents.*	ω_r	Rotor speed.
$V_{s\alpha}$ $V_{s\beta}$	*α and β components of stator voltage.*	T_e	Electromagnetic torque.
ψ_{sa} $\psi_{s\beta}$	*α and β components of stator flux.*	T_L	Load torque.
ψ_{ra} $\psi_{r\beta}$	*α and β components of rotor flux*	V	Lyapunov function.
R_s R_r	*Stator and rotor resistances*	s	Laplace operator.
L_s L_r	*Stator and rotor inductances*	S	Sliding mode surface.
T_s T_r	*Stator and rotor time constants.*	K	Sliding mode controller gain.
σ	*Leakage coefficient.*	*OLSE*	Open Loop Speed Estimator.
M_{sr}	*Stator-rotor mutual inductance.*	*MRAS*	Model Reference Adaptive System
ω_r	*Angular velocity.*	*RTI*	Real Time interface.
K_p, K_i	*Proportional and integral gains of the PI controller*		

2 Induction machine mathematical model

The dynamic equations of the induction motor are given in (1) in the stationary reference frame:

$$\begin{cases} \dfrac{di_{s\alpha}}{dt} = -\left(\dfrac{R_s}{\sigma L_s} + \dfrac{R_r}{\sigma L_r}\right) i_{s\alpha} - \omega_r i_{s\beta} + \dfrac{R_s}{\sigma L_s L_r}\psi_{s\alpha} + \dfrac{\omega_r}{\sigma L_r}\psi_{s\beta} + \dfrac{1}{\sigma L_s} V_{s\alpha} \\ \dfrac{di_{s\beta}}{dt} = -\left(\dfrac{R_s}{\sigma L_s} + \dfrac{R_r}{\sigma L_r}\right) i_{s\beta} + \omega_r i_{s\alpha} + \dfrac{R_s}{\sigma L_s L_r}\psi_{s\beta} - \dfrac{\omega_r}{\sigma L_r}\psi_{s\alpha} + \dfrac{1}{\sigma L_s} V_{s\beta} \\ \dfrac{d\psi_{s\alpha}}{dt} = V_{s\alpha} - R_s i_{s\alpha} \\ \dfrac{d\psi_{s\beta}}{dt} = V_{s\beta} - R_s i_{s\beta} \\ \dfrac{d\omega_r}{dt} = \dfrac{1}{J}(T_e - T_L) - \dfrac{f_r \omega_r}{J} \end{cases} \quad (1)$$

Knowing that $\sigma = 1 - \dfrac{M_{sr}}{L_s L_r}$ is leakage coefficient.

J and f_r are the inertia moment and the friction coefficient respectively.

The electromagnetic torque is expressed by:

$$T_e = p(\psi_{s\alpha} i_{s\beta} - \psi_{s\beta} i_{s\alpha}) \quad (2)$$

3 Sliding mode observer design for flux and speed estimation

The Sliding mode observers provide high effectiveness due to a number of advantages such as high robustness, simple implementation and reduced computation requirements. The proposed SMO design in this work does not employ the speed

adaptation scheme [22]. Contrary to the conventional adaptive observers, this observer means does not take the rotor speed as an adaptive quantity, where the speed estimator is separated completely from the main observer. This increases the accuracy in a wide-speed-range operation and reduces the design complexity [23,24]

The SMO is based on the state model of induction motor. The presented IM in (1) can be written in complex from as the following:

$$\begin{cases} \dfrac{\mathrm{d}\bar{\psi}_s}{\mathrm{d}t} = R_s\bar{i}_s - j\,\omega_r + \bar{V}_s \\ \dfrac{\mathrm{d}\bar{i}_s}{\mathrm{d}t} = -\left(\dfrac{R_s}{\sigma L_s} + \dfrac{R_r}{\sigma L_r}\right) i_s + \dfrac{1}{\sigma L_s}\left(\dfrac{R_r}{L_r} - j\,\omega_r\right)\bar{\psi}_s + \dfrac{1}{\sigma L_s}\bar{V}_s \end{cases} \tag{3}$$

In this observer, the back-emf terms $(\omega_r\psi_s)$ are considered as disturbances. Then, the model of observer being shown in Fig.1 can be expressed as follows:

$$\begin{cases} \dfrac{\mathrm{d}\hat{\bar{\psi}}_s}{\mathrm{d}t} = R_s\bar{i}_s + \bar{V}_s - K\,\mathrm{sign}(S_{\bar{i}_s}) \\ \dfrac{d\hat{\bar{i}}_s}{dt} = -\left(\dfrac{R_s}{\sigma L_s} + \dfrac{R_r}{\sigma L_r}\right)\bar{i}_s + \dfrac{R_r}{\sigma L_s L_r}\hat{\bar{\psi}}_s + \dfrac{1}{\sigma L_s}\bar{V}_s - \dfrac{1}{\sigma L_s}K\,\mathrm{sign}(S_{\bar{i}_s}) \end{cases} \tag{4}$$

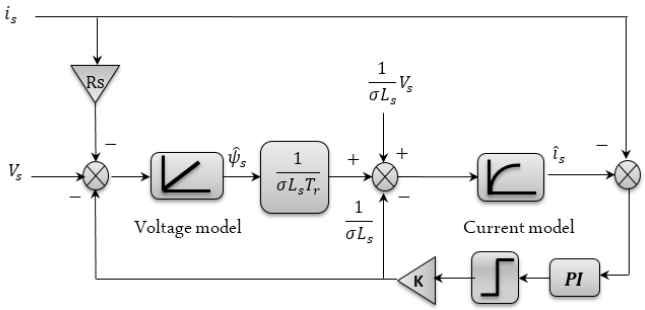

Fig.1 Sliding mode stator flux observer

With

K is the sliding mode switching gain.

S_i is the sliding surface of the current error.

In the SMO, the traditional *sign* function is replaced by a softer function related to sigmoid function *sigm(S)* to reduce the chattering effect

$$sigm\,(S) = \left(\frac{2}{1+\mathrm{e}^{\delta S}}\right) - 1 \tag{5}$$

δ is a small positive constant which adjusts the sigmoid function slope.

The PI controller is added just to impose faster desired error convergence, where the sliding surface is given by:

$$S_{i_s} = \left(K_{\mathrm{p}} + \frac{K_{\mathrm{i}}}{s} \right) \left(\hat{i}_{\mathrm{s}} - i_{\mathrm{s}} \right) \tag{6}$$

By using Lyapunov candidate function and IM and SMO models presented in (3) and (4), the gain K can be given as:

$$K > \max \left(\left| \omega_{\mathrm{r}} \psi_{\mathrm{s}} - \hat{e}_{\psi_s} / T_r \right| \right) \tag{7}$$

where $\hat{e}_{\psi_s}$ is the flux estimation error.

$$\hat{e}_{\psi_s} = \bar{\psi}_{\mathrm{s}} - \hat{\bar{\psi}}_{\mathrm{s}} \tag{8}$$

The advantage of this SMO is that the rotor speed quantity is unrelated with observer design and when it is needed it can be computed easily by the following open-loop speed estimator (OLSE) expression:

$$\hat{\omega}_{\mathrm{r}} = \hat{\omega}_{\mathrm{s}} - \hat{\omega}_{\mathrm{sl}} = \frac{1}{{\psi_{\mathrm{r}}}^2} \left(\frac{\mathrm{d}\hat{\psi}_{\mathrm{r}\beta}}{\mathrm{d}t} \hat{\psi}_{\mathrm{r}\alpha} - \frac{\mathrm{d}\hat{\psi}_{\mathrm{r}\alpha}}{\mathrm{d}t} \hat{\psi}_{\mathrm{r}\beta} \right) - \frac{R_{\mathrm{s}} \hat{T_{\mathrm{e}}}}{p {\psi_{\mathrm{r}}}^2}. \tag{9}$$

ω_s, ω_{sl} are the stator magnetic field and slip angular velocities respectively.

4 Proposed stator flux-MRAS association for speed estimation

In practice, the measured signals mostly contain noises. Besides, the sensors themselves introduce a DC-offset that can saturate the integrators employed in the estimations [26]. However, the simulation shows a smooth estimation and no filtering is actually needed. The main drawback of the open loop speed estimator (OLSE) from the last section is the need of low pass filter is speed estimation process because that the computation of the rotor flux derivative is sensitive to noise. The use of LPF in the experimental implementation adds a delay in the feedback portion of the control system. Moreover, for excessive filtering, the system has been driven to instability, especially at low speeds.

In this section, the proposed scheme is a combination of SMO and MRAS theory, where the open-loop estimator is substituted by a model reference adaptive system (MRAS) for speed estimation. The classical structure of MRAS observer contains two parts, the reference model and the adaptive model, in addition to the adaptation mechanism [27]. In this work, the proposed modification consists in using the previous sliding mode observer as a reference model in MRAS, Then, the estimated flux quantities will be compared to those estimated by the adaptive model for speed computation. The presented MRAS design in this work focuses on a stator flux model instead of the rotor flux model in order to be more suitable for the DTC control algorithm.

The estimated flux components through the sliding mode observer are considered as a reference model:

$$\begin{cases} \hat{\psi}_{s\alpha} = \int \left(R_{\mathrm{s}} i_{\mathrm{s}\alpha} + V_{\mathrm{s}\alpha} - K \mathrm{sign}(S_{i_{s\alpha}}) \right) \\ \hat{\psi}_{s\beta} = \int \left(R_{\mathrm{s}} i_{\mathrm{s}\beta} + V_{\mathrm{s}\beta} - K \mathrm{sign}(S_{i_{s\beta}}) \right) \end{cases} \tag{10}$$

The adjustable model is expressed as follows:

$$\begin{cases} \tilde{\psi}_{s\alpha} = \dfrac{L_r}{R_r + L_r s}\left(\sigma L_s \hat{\omega}_r i_{s\beta} + \dfrac{L_s}{L_r}\left(R_r + \sigma L_r s\right) i_{s\alpha} - \hat{\omega}_r \tilde{\psi}_{s\beta} \right) \\ \tilde{\psi}_{s\beta} = \dfrac{L_r}{R_r + L_r s}\left(\sigma L_s \hat{\omega}_r i_{s\alpha} + \dfrac{L_s}{L_r}\left(R_r + \sigma L_r s\right) i_{s\beta} - \hat{\omega}_r \tilde{\psi}_{s\alpha} \right) \end{cases} \tag{11}$$

The error between the reference and the adaptive mode can be given by:

$$\begin{cases} \varepsilon_\alpha = \hat{\psi}_{s\alpha} - \tilde{\psi}_{s\alpha} \\ \varepsilon_\beta = \hat{\psi}_{s\beta} - \tilde{\psi}_{s\beta} \end{cases} \tag{12}$$

The error in (12) is used to drive a suitable adaptation mechanism to generates the estimated speed quantity [28]. By subtracting the adjustable model from the those obtained by the sliding mode observer, we obtain the following state error equations:

$$\begin{bmatrix} \dot{\varepsilon}_\alpha \\ \dot{\varepsilon}_\beta \end{bmatrix} = \begin{bmatrix} -\dfrac{1}{T_r} & -\omega_r \\ \omega_r & -\dfrac{1}{T_r} \end{bmatrix} \begin{bmatrix} \varepsilon_\alpha \\ \varepsilon_\beta \end{bmatrix} + \begin{bmatrix} -\hat{\psi}_{s\beta} & \sigma L_s i_{s\beta} \\ \hat{\psi}_{s\beta} & -\sigma L_s i_{s\alpha} \end{bmatrix} \left(\omega_r - \hat{\omega}_r\right) \tag{13}$$

Then, (13) can be written as:

$$[\dot{\varepsilon}] = [A][\varepsilon] + [W] \tag{14}$$

The hyperstability of the system is assured if the transfer matrix in the forward path of the is strictly real positive and the non-linear block in the feedback path satisfies Popov's criterion [25,28].

Popov's criterion requires:

$$\int_0^t [\varepsilon]^T [W] dt \geq \gamma^2 \tag{15}$$

with

$t \geq 0$ and γ is a positive constant.

The error function ε has the form of a vector inner product that is independent to the reference frame in which the vectors are expressed. It may be represented by the following linearized expression:

$$\varepsilon = \left(\hat{\psi}_{s\beta} \tilde{\psi}_{s\alpha} - \hat{\psi}_{s\alpha} \tilde{\psi}_{s\beta} - \left(i_{s\alpha} \varepsilon_\beta - i_{s\beta} \varepsilon_\alpha \right) \sigma L_s \right) \tag{16}$$

Finally, the motor speed is estimated as:

$$\hat{\omega}_r = K_p \varepsilon + K_i \int \varepsilon dt \tag{17}$$

The final form of the associated MRAS-Sliding mode observer is given in the following complex form:

$$\begin{cases} \dfrac{\mathrm{d}\hat{\bar{\psi}}_s}{\mathrm{d}t} = R_s \bar{i}_s + \bar{V}_s - K\,\mathrm{sign}(S_{\bar{i}_s}) \\ \dfrac{d\hat{\bar{i}}_s}{dt} = -\left(\dfrac{R_s}{\sigma L_s} + \dfrac{R_r}{\sigma L_r}\right)\bar{i}_s + \dfrac{R_r}{\sigma L_s}\hat{\bar{\psi}}_s + \dfrac{1}{\sigma L_s}\bar{V}_s - \dfrac{1}{\sigma L_s}K\,\mathrm{sign}(S_{\bar{i}_s}) \\ \hat{\omega}_r = K_p\,\dot{\varepsilon} + K_i\,\varepsilon \end{cases} \tag{18}$$

The block diagram of the association of MRAS estimator with SMO is presented in Fig.2.

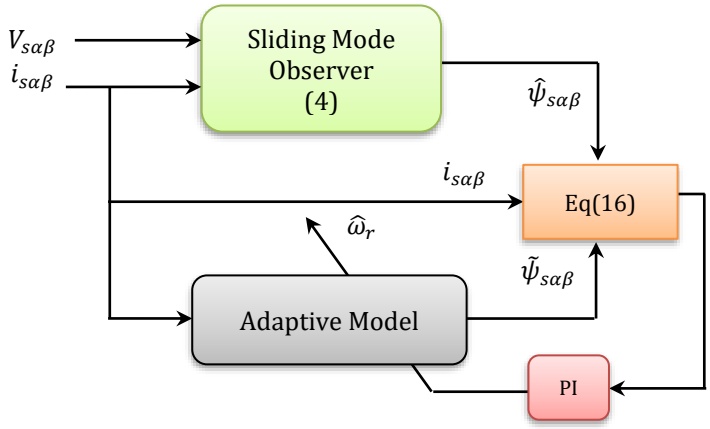

Fig.2 Association of Stator Flux model-MRAS speed observer with SMO.

5 Sensorless control design for induction motor based on feedback linearization and MRAS-SMO

5.1 Direct flux and torque control design using feedback linearization

In this section, the feedback linearization direct flux and torque control is proposed as a main control configuration. This method uses an inverse transformation to obtain the desired control for the original nonlinear system and achieve a decoupled flux and torque control [12]. This feedback linearization is considered as presented in [6,10], where, the assumed system outputs are the electromagnetic torque and the square of stator flux magnitude.

The control objectives are defined as:

$$\begin{cases} T_e = p(\psi_{s\alpha} i_{s\beta} - \psi_{s\beta} i_{s\alpha}) \\ |\psi_s|^2 = {\psi_{s\alpha}}^2 + {\psi_{s\beta}}^2 \end{cases} \tag{19}$$

$$\begin{cases} e_{T_e} = {T_e}^* - T_e \\ e_{\psi_s} = |\psi_s^*|^2 - |\psi_s|^2 \end{cases} \tag{20}$$

With:

e_{Te}, $e_{\psi s}$: torque and flux tracking errors.

Using the IM model presented in (1), the relationship between the input and the output can be found using the presented model as:

$$\dot{\mathbf{e}} = \begin{bmatrix} \dot{e}_{T_e} \\ \dot{e}_{\psi_s} \end{bmatrix} = \begin{bmatrix} F_1 \\ F_2 \end{bmatrix} + \mathbf{C}(x) \begin{bmatrix} V_{s\alpha}^* \\ V_{s\beta}^* \end{bmatrix} \tag{21}$$

With:

$$\begin{cases} F_1 = -p[\mu(\psi_{s\alpha} i_{s\beta} - \psi_{s\beta} i_{s\alpha}) + \omega_r (\psi_{s\alpha} i_{s\alpha} - \psi_{s\beta} i_{s\beta}) - \dfrac{\omega_r}{\sigma L_s} |\psi_s|^2] \\ F_2 = 2R_s (\psi_{s\alpha} i_{s\alpha} - \psi_{s\beta} i_{s\beta}) \end{cases}$$

$$\mathbf{C}(x) = \begin{bmatrix} -p\left(i_{s\beta} - \dfrac{\psi_{s\beta}}{\sigma L_s}\right) & p\left(i_{s\alpha} - \dfrac{\psi_{s\alpha}}{\sigma L_s}\right) \\ -2\psi_{s\alpha} & 2\psi_{s\beta} \end{bmatrix}$$

$V_{s\alpha}^*$, $V_{s\beta}^*$ are the reference voltage components.

The determinant of the matrix **C**(x) is computed as follows:

$$\det(\mathbf{C(x)}) = p \frac{M_{sr}}{\sigma L_s L_r} [\psi_{s\beta}\psi_{r\beta} + \psi_{s\alpha}\psi_{r\alpha}] \tag{22}$$

where:
$\psi_{r\alpha}$, $\psi_{r\beta}$ are rotor flux components.

As long as matrix **C**(x) is a non-singular, the system is said to be linearizable [12]. Therefore, the desired dynamics can be imposed on it.

The input-output feedback linearized system will be expressed as:

$$\mathbf{V_s} = \begin{bmatrix} V_{s\alpha}^* \\ V_{s\beta}^* \end{bmatrix} = \mathbf{C^{-1}}(x) \begin{bmatrix} -F_1 + V_1 \\ -F_2 + V_2 \end{bmatrix} \tag{23}$$

V_1 and V_2 are assumed auxiliary inputs to ensure better tracking accuracy and reach the desired behavior for the stator flux magnitude and the torque.

$$\begin{cases} V_1 = -k_1 e_{T_e} \\ V_2 = -k_2 e_{\psi_s} \end{cases} \tag{24}$$

For positive values of k_1 and k_2, the asymptotic stability can be guaranteed and therefore the tracking errors will have an exponential convergence. The appropriate selection of these gains affects a lot on control performance [11].

The feedback linearization control law (23) can be rewritten as follows:

$$\mathbf{V_s} = \mathbf{C^{-1}(x)}(-\mathbf{F} + \mathbf{V_{aux}}) \tag{25}$$

with

$$\mathbf{F} = \begin{bmatrix} F_1 \\ F_2 \end{bmatrix} \text{ and } \mathbf{V_{aux}} = \begin{bmatrix} V_1 \\ V_2 \end{bmatrix}$$

The control law should be chosen to satisfy the Lyapunov stability's condition. Hence, the Lyapunov candidate function for MIMO systems is:

$$V = \frac{1}{2} e^T e \tag{26}$$

The time-derivative of Lyapunov function is given by:

$$\dot{V} = e^T \dot{e} \tag{27}$$

The stability condition $\dot{V} < 0$ has to be verified. By substituting (23) in the derivative of Lyapunov function we can obtain:

$$\dot{V} = e^T \begin{bmatrix} -k_1 & 0 \\ 0 & -k_2 \end{bmatrix} \begin{bmatrix} e_{T_e} \\ e_{\psi_s} \end{bmatrix} \tag{28}$$

and this results in the following:

$$\dot{V} = -k_1 e_{T_e}^2 - k_2 e_{\psi_s}^2 \tag{29}$$

For k_1 and k_2 being positive, the derivative $\dot{V}$ is always negative which guarantees an asymptotical convergence of errors to zero and subsequently ensures the stability of the control system.

5.2 Stability analysis of the closed-loop system

To implement the global control algorithm, the flux observer must is initialized firstly with initial conditions different from zero in order to avoid the singularity in the matrix **C(x)** [29]. Therefore, an offset of 0.005Wb is added to the estimated flux. Then, the measured speed and flux must be replaced by their equivalents estimated quantities in the feedback linearization controller (23) [18,30]. The estimated quantities are marked by the hat (^) sign:

$$\mathbf{V_s}\left(\hat{\psi}_s, \mathrm{i_s}, \hat{\omega}_r\right) = \begin{bmatrix} V_{s\alpha}^* \\ V_{s\beta}^* \end{bmatrix} = \mathbf{C^{-1}}\left(x\right) \begin{bmatrix} -F_1 + V_1 \\ -F_2 + V_2 \end{bmatrix} \tag{30}$$

With:

$$\begin{cases} F_1 = -p[\mu(\hat{\psi}_{s\alpha}\hat{i}_{s\beta} - \hat{\psi}_{s\beta}\hat{i}_{s\alpha}) + \hat{\omega}_r(\hat{\psi}_{s\alpha}\hat{i}_{s\alpha} - \hat{\psi}_{s\beta}\hat{i}_{s\beta}) - \dfrac{\hat{\omega}_r}{\sigma L_s}\left|\psi_s\right|^2] \\ F_2 = 2R_s(\hat{\psi}_{s\alpha}\hat{i}_{s\alpha} - \hat{\psi}_{s\beta}\hat{i}_{s\beta}) \end{cases}$$

$$\mathbf{C}\left(x\right) = \begin{bmatrix} -p\left(\hat{i}_{s\beta} - \dfrac{\hat{\psi}_{s\beta}}{\sigma L_s}\right) & p\left(\hat{i}_{s\alpha} - \dfrac{\hat{\psi}_{s\alpha}}{\sigma L_s}\right) \\ -2\hat{\psi}_{s\alpha} & 2\hat{\psi}_{s\beta} \end{bmatrix}$$

The torque and the flux tracking error can be given by:

$$\begin{cases} \hat{e}_{T_e} = T_e - \hat{T}_e\left(\hat{\psi}_s, \hat{\mathrm{i}}_s\right) \\ \hat{e}_{\psi_s} = \left|\psi_s\right|^2 - \left|\hat{\psi}_s\right|^2 \end{cases} \tag{31}$$

$$\hat{\mathbf{e}} = \begin{bmatrix} \hat{e}_{T_e} \\ \hat{e}_{\psi_s} \end{bmatrix} = \begin{bmatrix} F_1 \\ F_2 \end{bmatrix} + \mathbf{C}(x) \begin{bmatrix} V_{s\alpha}^* \\ V_{s\beta}^* \end{bmatrix} \tag{32}$$

By substituting (30) in (32), the controller dynamics become:

$$\begin{cases} \dot{\hat{e}}_{T_e} = -k_1 \hat{e}_{T_e} \left(\hat{\psi}_s , \hat{\mathrm{i}}_s \right) \\ \dot{\hat{e}}_{\psi_s} = -k_2 \hat{e}_{\psi_s} \end{cases} \tag{33}$$

Considering the dynamic errors given in (33), at $t = T_s$, the observer converges (i.e. $\hat{\psi}_s \to \psi_s$, $\hat{T_e} \to T_e$, $\hat{\omega}_r \to \omega_r$) and the estimation errors exponentially reaches to zero. Then, it can be proved that the real values of the stator flux and torque will also exponentially converge to their reference values.

Fig.3 shows the system configuration of the proposed sensorless control scheme using nonlinear IOFL-DTC with stator flux based MRAS-sliding Mode observer. For speed control an anti-windup PI controller is used. The space vector modulation (SVM) is considered for inverter switching control.

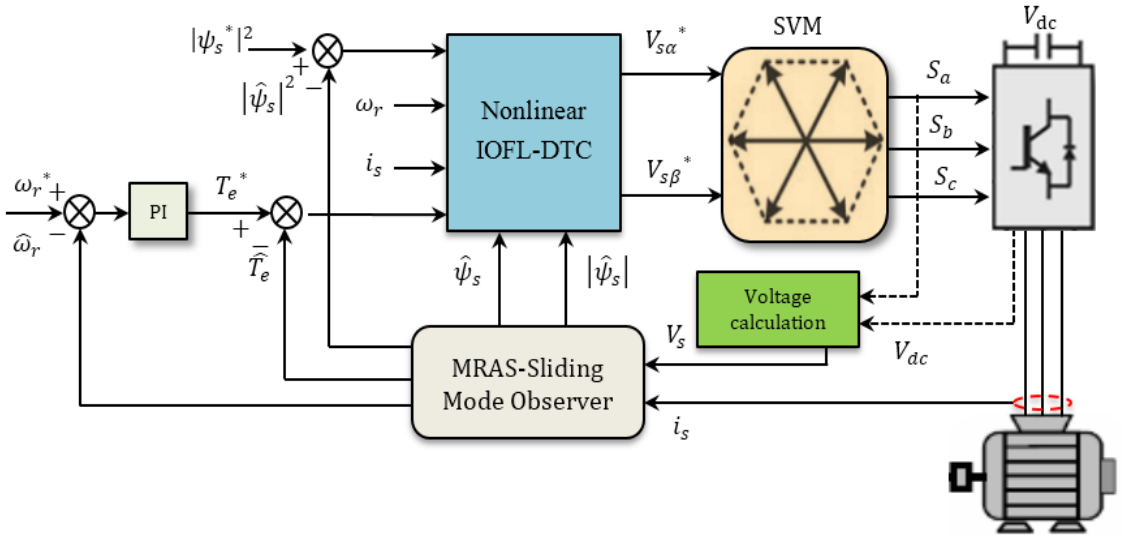

Fig.3 System configuration of sensorless direct torque control based on feedback linearization and MRAS-sliding mode observer.

6 Simulation results

The proposed control algorithm has been verified through numerous simulation tests using MATLAB/Simulink software. The considered machine for simulation and experimental implementation later is a three-phase 1.1 kW squirrel-cage induction motor, its parameters are given in the appendix section. The obtained simulation results investigate the performance of the feedback linearization based-direct torque control and the estimation accuracy of the associated MRAS-sliding mode observer (MRAS-SMO).

The proposed observer is compared with two other observer structures, a full-order adaptive observer as presented in [17] and basic sliding mode observer with open loop speed estimator (OLSE-SMO). The following figures present the estimated speed and estimation errors under different conditions without load application. (a) for the adaptive observer, (b) for the sliding mode observer with OLSE (OLSE-SMO) and (c) for the associated MRAS-sliding mode observer (MRAS-SMO).

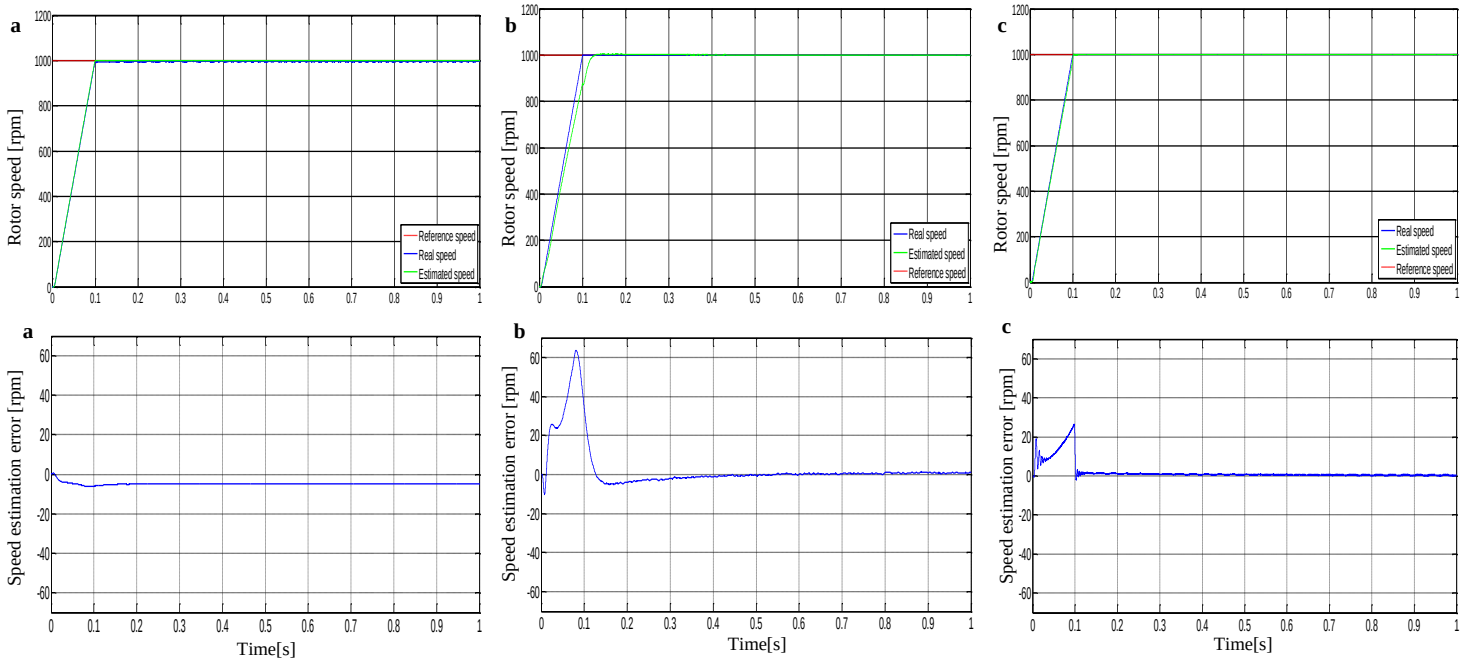

Fig.4 Starting and steady state operations: real and estimated rotor speeds with estimation error [rpm].

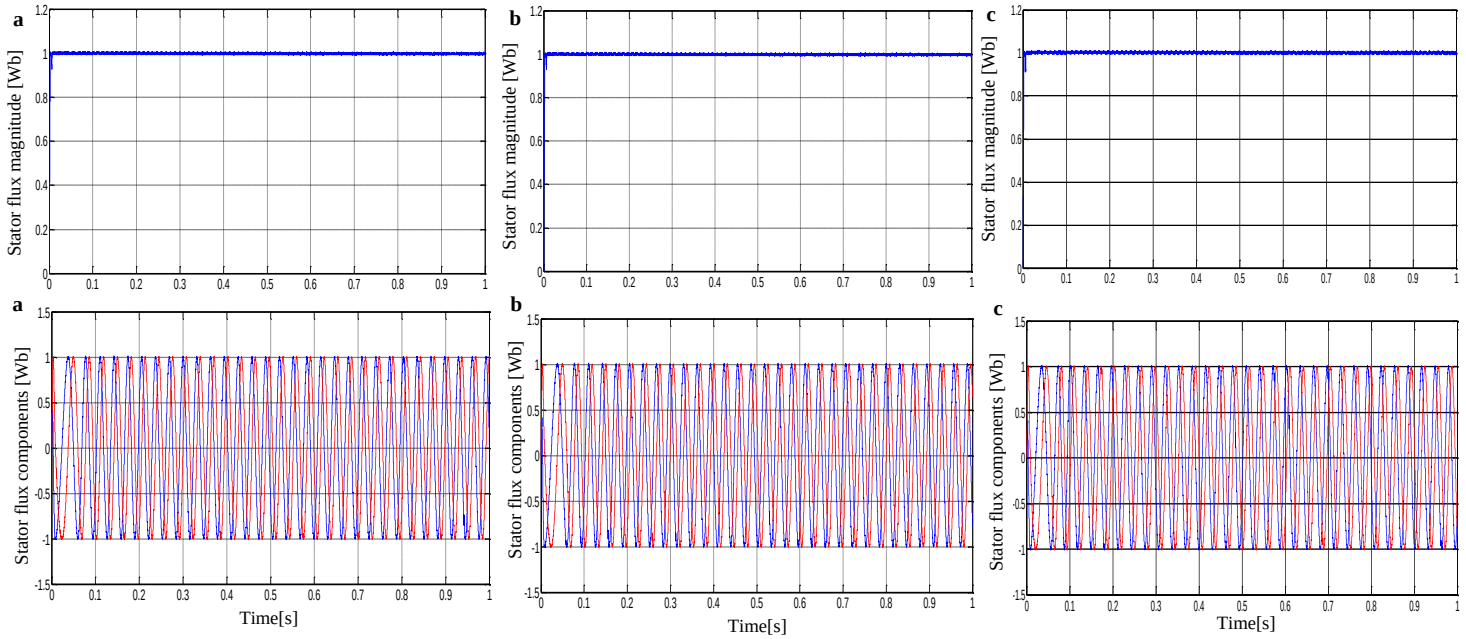

Fig.5 Estimated stator flux magnitude and components [Wb].

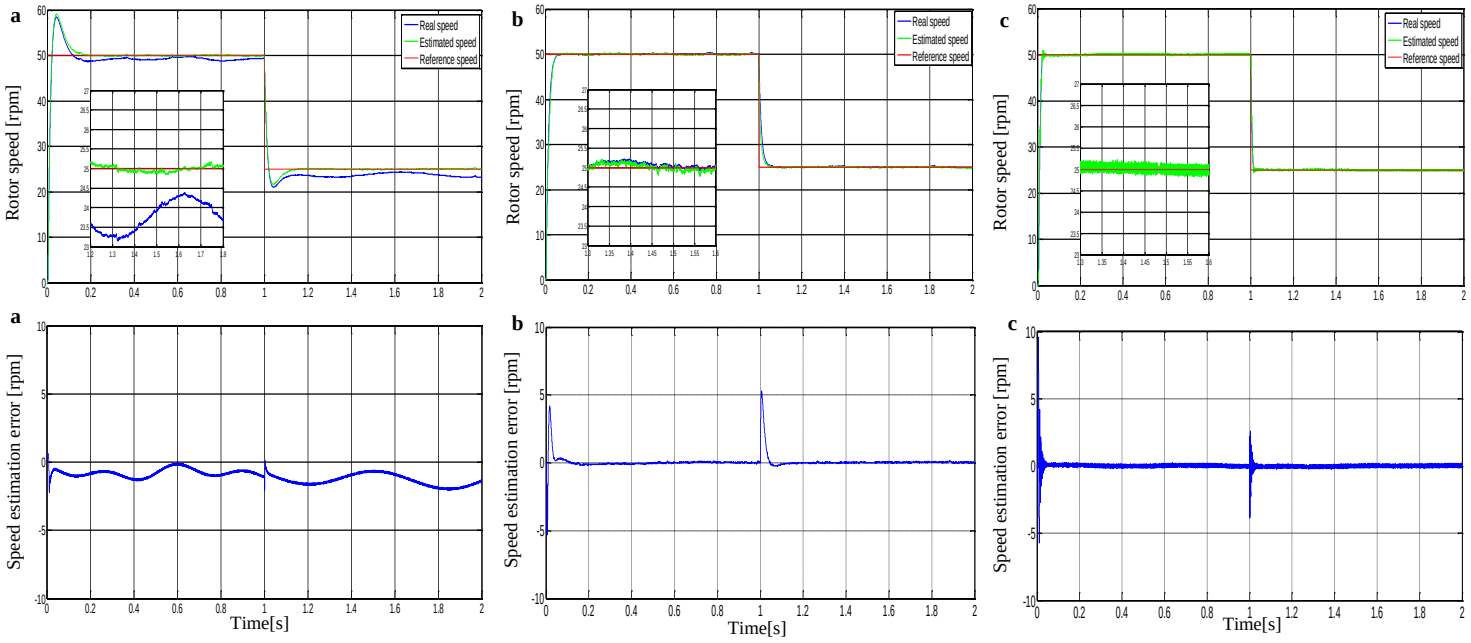

Fig.6 Real and estimated speeds at low speed operation with estimation error (*50 rpm;25 rpm*).

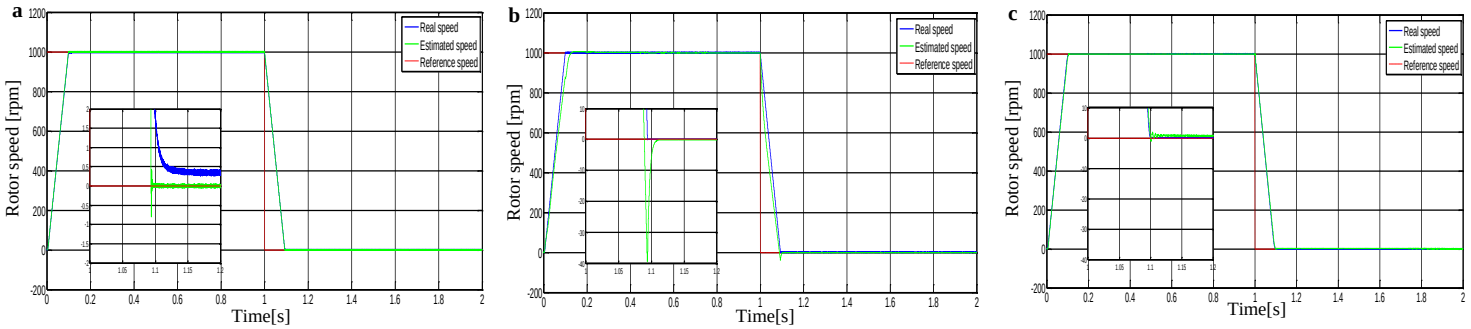

Fig.7 Real and estimated speeds under zero-speed operation test.

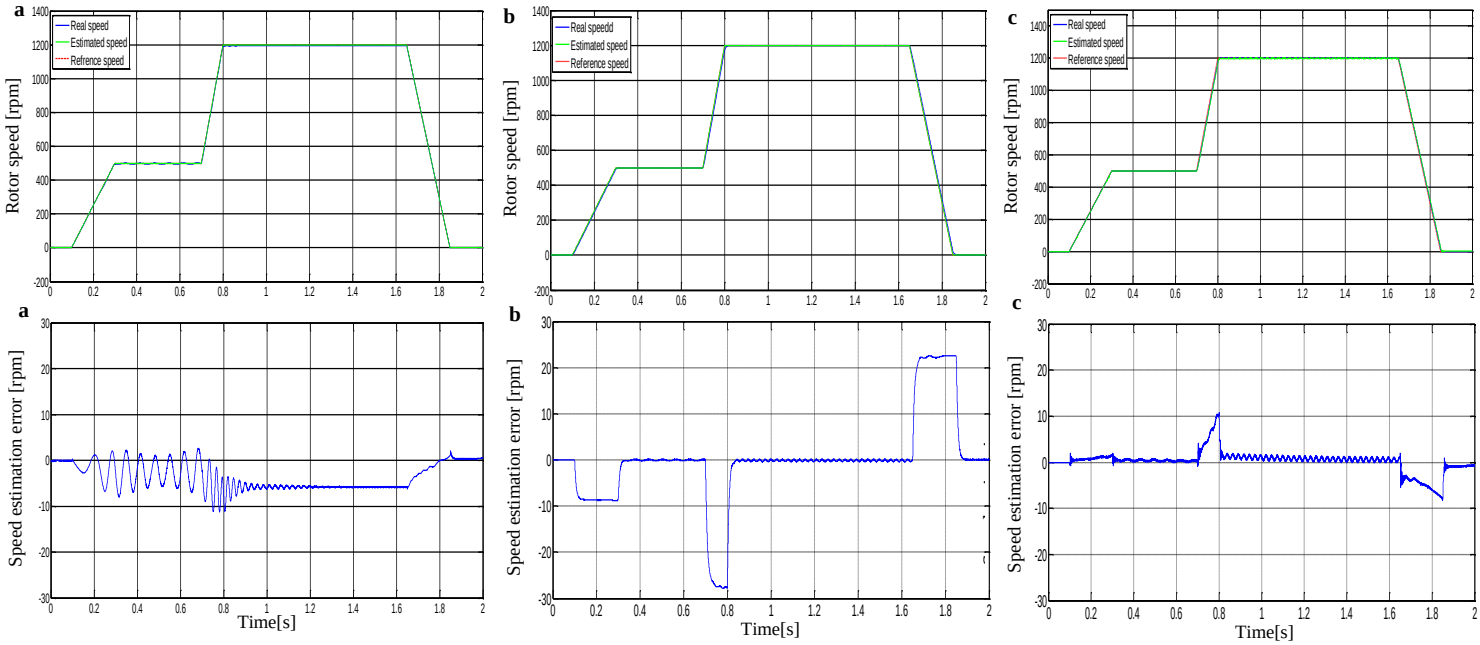

Fig.8 Real and estimated speeds under variable profile test with estimation error (benchmark).

Fig.4 illustrates the from top to bottom the motor speed response and estimation errors to the step input of (1000 rpm) without load. It can be seen that the estimated speed follows the real speed for all three observers. The adaptive observer in Fig.4(a) shows a good superposition between the real and estimated speed quantities in the transient state, while the OLSE-SMO shows better static error convergence in the steady state. Further, the association of MRAS-SMO provided better estimation accuracy and could eliminate the error in both transient and states. This can be more justified by comparing to the estimation errors which are depicted in the bottom of the Fig.4(a-b-c), it shows that the MRAS-SMO has the fastest convergence and the most minimized error than the other observers. In Fig.5, the estimated stator flux is shown. The figure presents the flux magnitude and axis components for the three observers. Since the stator flux magnitude is forced by the control algorithm, all observers show an accurate estimation and good waveform for stator flux.

Next, the low-speed operation simulation results are illustrated in Figs.6, where a speed variation from *50 rpm* to *25 rpm* has been conducted. It can be seen that the adaptive observer shows an important overshoot, unstable behavior and considerable error during the low-speed condition in Fig.6(a), as it can be seen that the OLSE-SMO shows an acceptable superposition between speed quantities with some fluctuations in Fig.6(b). However, it is clear from Fig.6(c) that the associated MRAS-SMO has better estimation and more precise superposition between speed quantities than the two previous observers. All these remarks can be confirmed from the estimation errors which displayed in the bottom of Fig.6(a-b-c). The zero-speed test's results are shown in Fig.7. The MRAS-SMO has better estimation accuracy during the speed variation compared to the adaptive observer and OLSE-SMO. At zero speed state, the proposed observer structure in Fig.7(c) has kept a correct estimation at zero speed/frequency values with reduced static error or overshoot.

The last test is presented in Figs.8, it evaluates the speed estimation under a variable speed reference profile (industrial benchmark). This test can comprise all the previous tests. Fig.8 shows the rotor speed estimation and estimation errors of all observers under a variable reference from zero to medium speed (*500 rpm*) to high-speed value (*1200 rpm*). It can be realized that the adaptive observer shows high error during the steady state in Fig.8(a), while the OLSE-SMO provides high estimation error at variable states and eliminates this error in the steady state in Fig.8(b). The MRAS based sliding mode observer in Fig.8(c) provides the best estimation and speed superposition during speed reference variations. Furthermore, it has provided the most reduced estimation error in dynamic state operation and very quick convergence in steady state. Table.1 summarizes and recapitulates the comparison in terms of speed estimation accuracy between the three observers.

Observer	Adaptive observer	OLSE-SMO	Associated MRAS-SMO
Static error (%)	≈ 0.5%	≈ 0.1%	≈ 0.06%
Dynamic error (%)	≈ 0.092%	≈ 0.25%	≈ 0.083%

Table.1 Comparative analysis between OLSE and MRAS based SM observers.

7 Experimental validation

The experimental results are obtained with the aid of software/hardware linking of MATLAB/Simulink/dSpace 1104 interface. The main components composing the experimental test rig of the proposed structure (Fig. 9) are: a squirrel-cage IM 1.1 kW (1), power electronics Semikron converter (2), position and speed sensor (incremental encoder type) being used to compare the measured speed with the estimated speed quantity (3). The proposed control algorithm is implemented using a dSpace dS 1104 controller (4) with the help of MATLAB/Simulink/Control desk software being plugged into a personal computer (5). The motor is associated with a magnetic powder brake to vary the load using a load control unit (6). Hall effect current sensors (7) are used to measure current while LEM voltage sensors (8) are used to measure voltage and both displayed on a digital scope (9).

The conducted tests in this section are the same as the considered tests in simulation section.

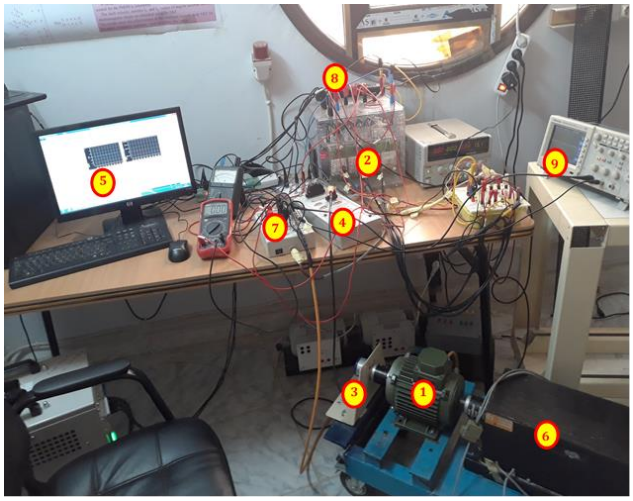

Fig.9 Test bench description.

Fig.10 shows a descriptive diagram of experimental setup and software/hardware linking. The dSpace 1104 board is an input-output (I/O) interface between the power electronics devices and the software part (i.e. MATLAB/Simulink). For each sampling period, the dS1104 receives the input signals from the different sensors (currents, voltages and rotor speed) and generates the digital control signals. These signals are provided by MATLAB/Simulink program with the real-time interface (RTI). The real-time interface gives the access to adjust all control variables in order to obtain a desirable behavior. The sampling frequency of dSpace 1104 can reach to 20 kHz. The suitable choice of sampling frequency has an apparent influence on quality of output signals.

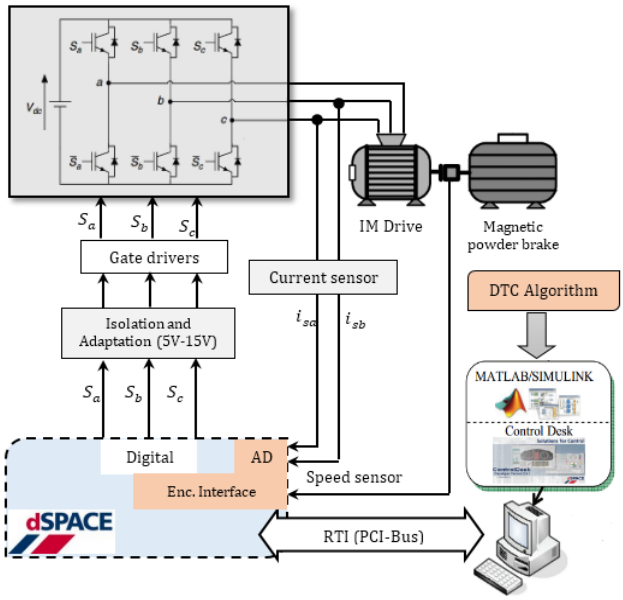

Fig.10 Descriptive block diagram of the dSpace based experimental setup.

The experimental results investigate the association of the feedback linearization-based DTC strategy with different sensorless algorithms (i.e. a: full order adaptive observer, b: sliding mode observer with open loop speed estimator (OLSE-SMO) and c: associated MRAS sliding mode observer (MRAS-SMO)) under the same previous conditions to validate the simulation results. The following figures present the speed estimation and estimation errors without load application.

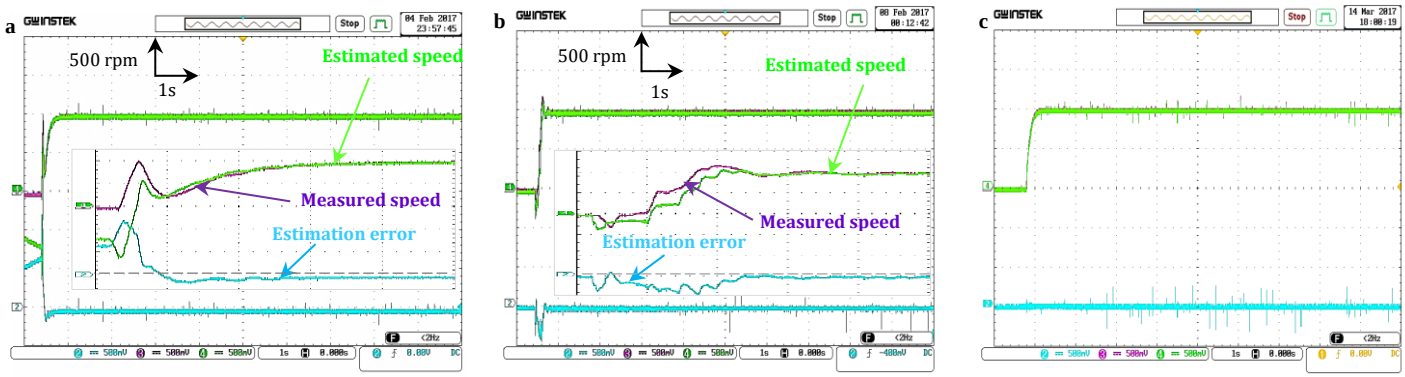

Fig.11 Motor starting and steady state operation: measured and estimated rotor speeds with estimation errors [rpm].

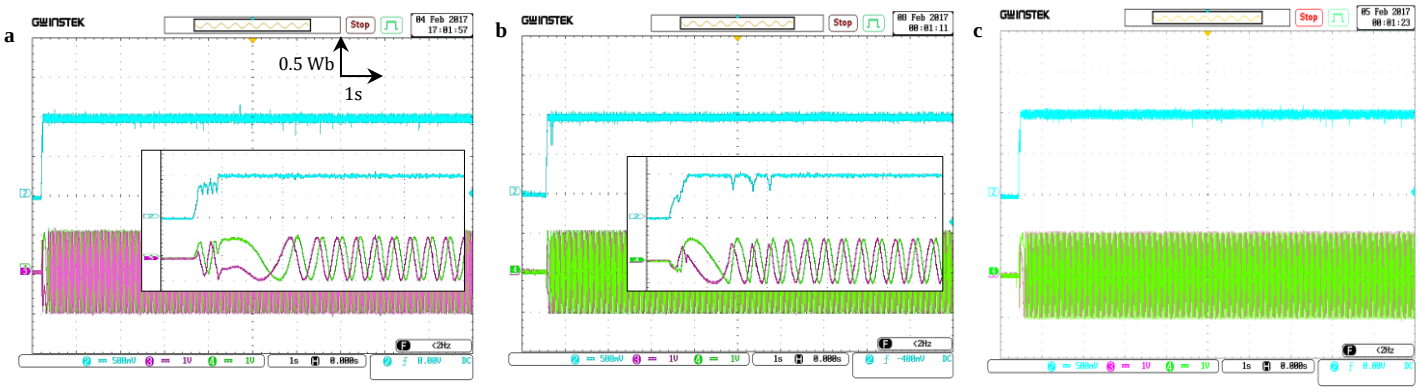

Fig.12 Estimated stator flux magnitude and components [Wb].

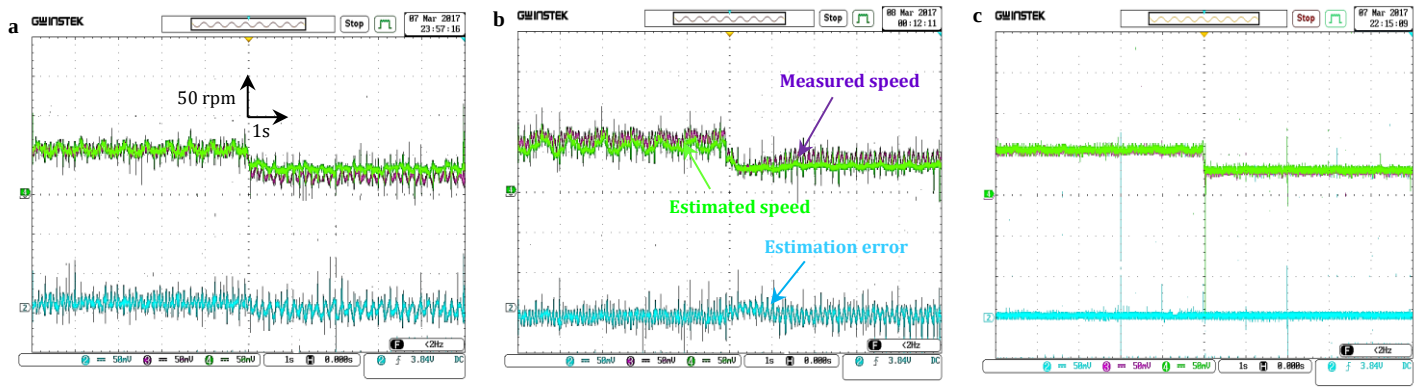

Fig.13 Measured and estimated speeds at low speed operation (*50 rpm;25 rpm*) with estimation errors.

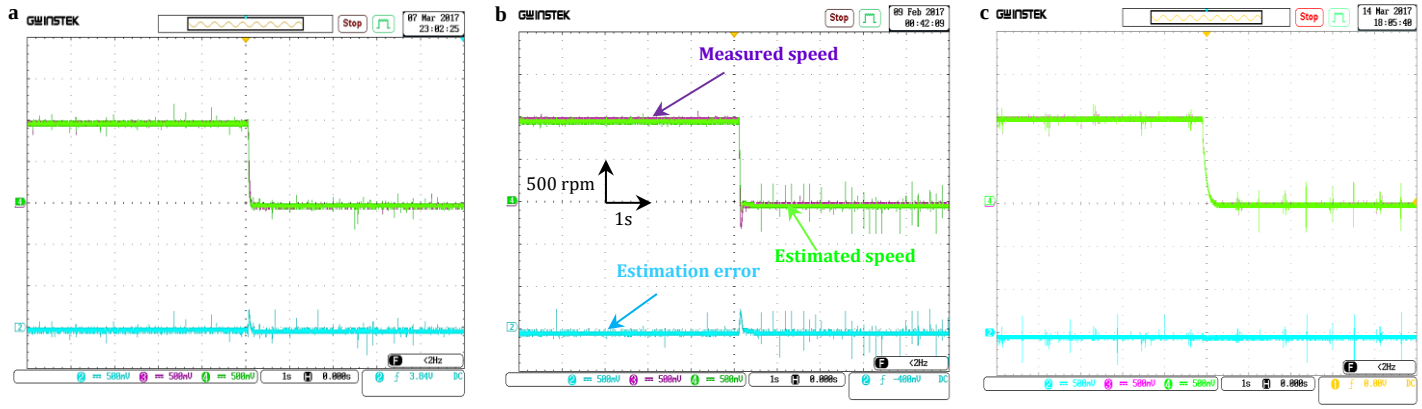

Fig.14 Measured and estimated speeds under zero-speed operation test with estimation errors.

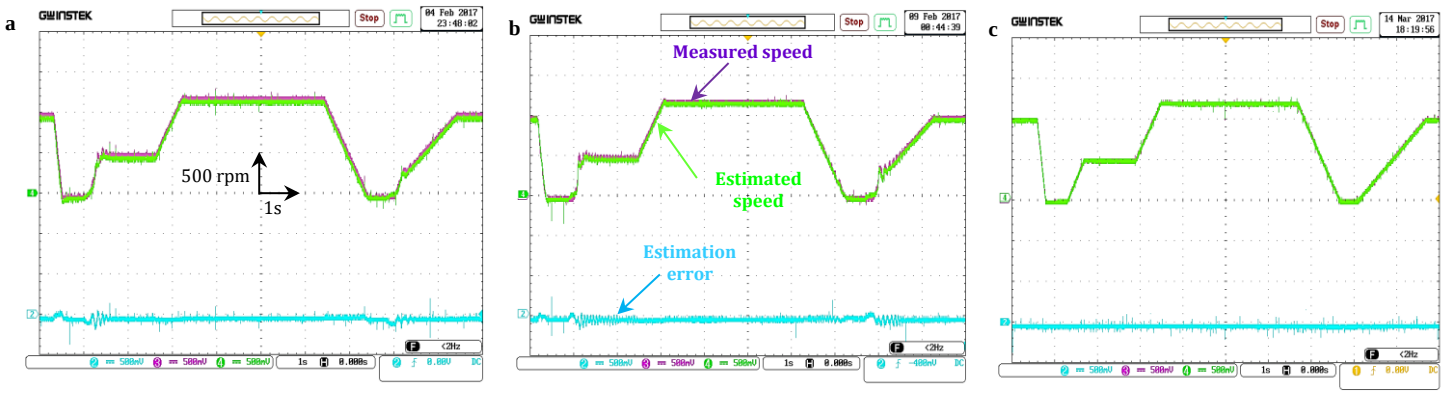

Fig.15 Measured and estimated speeds under variable profile test (benchmark) with estimation errors.

Fig.11 shows the rotor speed at the starting for the driven IOFL-DTC induction motor with three observers. The adaptive observer in (Fig.11(a), OLSE-SMO in (Fig.11(b)) and MRAS-SMO in Fig.11(c)). It can be observed that before the starting up instant, the adaptive observer has initial estimated speed and error values. This phenomenon has not arisen previously in simulation results, it is caused mainly by the measurement noise (Current and voltage sensors). Contrariwise, OLSE-SMO and MRAS-SMO have avoided this problem due the separated structure of speed estimator. It can be deduced also that MRAS-SMO provides smoother starting and better accuracy in the transient state compared to the OLSE-SMO observer which shows a considerable

overshoot. In addition, the static error has been minimized. Fig.12 illustrates the observed stator flux magnitude (*1div =0.5 Wb*) and its axes components (*1div =1 Wb*). The flux magnitude is forced by the control algorithm in closed loop, therefore, All observers show an accurate estimation and good waveform for stator flux.

Then, in Fig.13, a speed variation test has been conducted at very low speed values (*50 rpm to 25 rpm (≈2.61 rad/s*)), (*1div=50 rpm*). Fig.13 illustrates that the adaptive observer and OLSE-SMO suffer from high oscillations and instability in speed estimation owing to the sensitive nature of the speed estimation process. This phenomenon is clearly shown in experimental results compared to the simulation due to presence of real noises and offsets in acquired signals. In the other hand, one can see that the main improvement of using the MRAS-SMO (Fig.13(c)) is more evident when dealing with noises and offsets. In fact, MRAS has solved the problem of the sensitivity to noise of the SMO at low speed operations regions. The figure shows also that the estimated and the measured speed are in good agreement without altering stability and generating fluctuations.

The zero-speed test is presented in Fig.14. All observers show stable speed estimation at zero speed/frequency (*0 rmp;0 Hz*). The speed value is almost correct even when the machine stops rotation. Finally, the variable speed profile (benchmark) test is illustrated in Fig.15. This test summarizes all the previous speed tests. It can be seen that the obtained result looks the same with those obtained with the same test in simulation section. The adaptive observer manifests a minor error during the instantaneous variation of speed but it could not minimize this error in the steady state, whilst, the OLSE-SMO manifests some fluctuations and errors during the variation of speed. The associated MRAS-SMO in Fig.15 (c) shows perfect superposition and reduced error between speed quantities. Furthermore, it is more stable during speed variation compared to the other two observes in Fig.15 (a-b). As a matter of fact, different problems arise in the experimental phase of the sensorless control that were not present in the simulation phase. This is due to the ideality of modeling and the absence of measurement noises or other influential factors. One can understand that the real limits of the adaptive observer and SMO with the open loop speed estimator appear in the real implementation.

As a summary, the SMO presents a better estimation than the adaptive full order in most of the tests in the steady state due to its inherent structure. Some problems appear in the experimental results at low speeds (oscillation and inaccuracy) due to high sensitivity of speed estimator to noise. The proposed solution for SMO performance improvement by the conjunction of MRAS combines the advantages of both algorithms and provides a more accurate estimation.

8 Conclusion

This paper has presented a new sensorless control algorithm for performance enhancement for direct torque control driven induction motor. The proposed algorithm consists of the association of the feedback linearization-based controller to a combined MRAS-Sliding mode observer. The decoupled flux and torque control has been achieved using feedback linearization approach which generates appropriate reference voltages. While various sensorless algorithms have been designed for flux and speed

reconstruction. The simulation and experimental results have been retrieved using dSpace 1104 board. Different tests have been conducted to check the control stability and robustness and the estimation accuracy of the different observers, such as starting up, at the low-speed range and with variable speed profile (i.e. benchmark trajectory). The use of nonlinear control strategy instead of linear controllers has given better advantages like a fast response, simplicity in control application and good reference tracking in different operation conditions. However, several problems have been shown during the experimental implementation due to sensorless control. In particular, at low speeds due to the presence of measurement noises, filter delays and many other influential factors. For this reason, a proposed structure has been presented to improve the performance of the SMO. An MRAS estimator is injected to replace the open-loop estimator in order to improve speed estimation and to reduce observer sensitivity, especially in very low regions.

The results show that the traditional observer structures show high sensitivity and important errors at low-speed tests, while the MRAS-SMO has kept its good accuracy and smooth response. Besides, the industrial benchmark test, prove the weakness of the adaptive observer and OLSE-SMO in variable states. Contrariwise, the MRAS-SMO has a perfect speed quantities superposition. In general, the combination of a nonlinear control algorithm with DTC principles can solve the traditional control problems. Moreover, the conjunction of MRAS with SMO as a sensorless speed estimation algorithm preserves high accuracy and stability even in hard condition. That is, it can improve comprehensively the performance of the sensorless drives.

Appendix

The parameters of the three-phase Induction motor, employed for the simulation and the experimental implementation, in SI units are:

Machine's Power	P = 1.1 kW
Rated voltage	V_s = 230/400 V
Rated current	I = 2.5 A
Rated stator flux	ψ_s = 0.95 Wb
Rated Torque	T_e = 6 N·m
Rated speed	ω_r = 1450 rpm
Frequency	f = 50 Hz
Stator resistance	R_s = 6.75 Ω
Rotor resistance	R_r = 6.21 Ω
Stator inductance	L_s = 0.5192H
Rotor inductance	L_r =0.5192H
Mutual inductance	M_{sr}= 0.4957 H
Number of pole pairs	p=2
Friction coefficient	f_r=0.002 N·m·s
The moment of inertia	J = 0.01240 kg·m^2
Inverter DC-link capacitor	C = 2040 μF

Table.2 Induction machine characteristics

The different control gains of simulation and experimental implementation:

Gains	Values
PI speed controller	K_p= 0.1; K_i= 0.234
Feedback linearization controllers	k_1=8000; k_2= 8000
Sliding mode flux observer gains	K = 2000
Sliding mode flux observer PI controller	K_p = 1; K_i = 1000
MRAS Adaptation mechanism PI controller	K_p = 85; K_i = 2000

Table.3 control gains and parameters

References

[1] Casadei D, Profumo F, Serra G, Tani A. FOC and DTC: Two viable schemes for induction motors torque control. IEEE Trans Power Electron 2002;17:779–87. doi:10.1109/TPEL.2002.802183.

[2] Lascu C, Trzynadlowski AM. Combining the Principles of Sliding Mode, Direct Torque Control, and Space-Vector Modulation in a High-Performance Sensorless AC Drive. IEEE Trans Ind Appl 2004;40:170–7. doi:10.1109/TIA.2003.821667.

[3] Attique QM. A Survey on Space-Vector Pulse Width Modulation for Multilevel Inverters. CPSS Trans Power Electron Appl 2017;2:226–36. doi:10.24295/CPSSTPEA.2017.00021.

[4] Saberi H, Feyzi M, Sharifian MBB, Sabahi M. Improved sensorless direct torque control method using adaptive flux observer. IET Power Electron 2014;7:1675–84. doi:10.1049/iet-pel.2013.0390.

[5] Liu X, Yu H, Yu J, Zhao L. Combined Speed and Current Terminal Sliding Mode Control With Nonlinear Disturbance Observer for PMSM Drive. IEEE Access 2018;6:29594–601. doi:10.1109/ACCESS.2018.2840521.

[6] Ammar A. Performance improvement of direct torque control for induction motor drive via fuzzy logic-feedback linearization. COMPEL - Int J Comput Math Electr Electron Eng 2019:COMPEL-04-2018-0183. doi:10.1108/COMPEL-04-2018-0183.

[7] Lascu C, Jafarzadeh S, Fadali MS, Blaabjerg F. Direct Torque Control With Feedback Linearization for Induction Motor Drives. IEEE Trans Power Electron 2017;32:2072–80. doi:10.1109/TPEL.2016.2564943.

[8] Lozada-Castillo N, Luviano-Juárez A, Chairez I. Robust control of uncertain feedback linearizable systems based on adaptive disturbance estimation. ISA Trans 2019;87:1–9. doi:10.1016/j.isatra.2018.10.003.

[9] Yazdanpanah R, Soltani J, Arab Markadeh GR. Nonlinear torque and stator flux controller for induction motor drive based on adaptive input–output feedback linearization and sliding mode control. Energy Convers Manag 2008;49:541–50. doi:10.1016/j.enconman.2007.08.003.

[10] Ammar A, Bourek A, Benakcha A. Nonlinear SVM-DTC for induction motor drive using input-output feedback linearization and high order sliding mode control. ISA Trans 2017;67:428–42. doi:10.1016/j.isatra.2017.01.010.

[11] Choi Y-S, Choi HH, Jung J-W. Feedback Linearization Direct Torque Control With Reduced Torque and Flux Ripples for IPMSM Drives. IEEE Trans Power Electron 2016;31:3728–37. doi:10.1109/TPEL.2015.2460249.

[12] Zhang Z, Tang R, Bai B, Xie D. Novel Direct Torque Control Based on Space Vector Modulation With Adaptive Stator Flux Observer for Induction Motors. IEEE Trans Magn 2010;46:3133–6. doi:10.1109/TMAG.2010.2051142.

[13] Accetta A, Ieee M, Alonge F, Ieee M, Cirrincione M, Ieee SM, et al. Robust control for high performance induction motor drives based on partial state-feedback linearization. IEEE Trans Ind Appl 2018;PP:1. doi:10.1109/TIA.2018.2869112.

[14] Gómez-Peñate S, Valencia-Palomo G, López-Estrada F, Astorga-Zaragoza C, Osornio-Rios RA, Santos-Ruiz I. Sensor Fault Diagnosis Based on a Sliding Mode and Unknown Input Observer for Takagi-Sugeno Systems with Uncertain Premise Variables. Asian J Control 2019;21:339–53. doi:10.1002/asjc.1913.

[15] Salim R, Mansouri A, Bendiabdellah A, Chekroun S, Touam M. Sensorless passivity based control for induction motor via an adaptive observer. ISA Trans 2018. doi:10.1016/j.isatra.2018.10.002.

[16] Barut M, Bogosyan S, Gokasan M. Speed-Sensorless Estimation for Induction Motors Using Extended Kalman Filters. IEEE Trans Ind Electron 2007;54:272–80. doi:10.1109/TIE.2006.885123.

[17] Pimkumwong N, Wang M. Full-order observer for direct torque control of induction motor based on constant V/F control technique. ISA Trans 2018;73:189–200. doi:10.1016/j.isatra.2017.12.014.

[18] Ghanes M, Gang Zheng. On Sensorless Induction Motor Drives: Sliding-Mode Observer and Output Feedback Controller. IEEE Trans Ind Electron 2009;56:3404–13. doi:10.1109/TIE.2009.2026387.

[19] Ye S. Fuzzy sliding mode observer with dual SOGI-FLL in sensorless control of PMSM drives. ISA Trans 2019;85:161–76. doi:10.1016/j.isatra.2018.10.004.

[20] Ammar A, Bourek A, Benakcha A. Sensorless SVM-Direct Torque Control for Induction Motor Drive Using Sliding Mode Observers. J Control Autom Electr Syst 2017;28:189–202. doi:10.1007/s40313-016-0294-7.

[21] Trabelsi R, Khedher A, Faouzi M, Faouzi M. Backstepping control for an induction motor using an adaptive sliding rotor-flux observer. Electr Power Syst Res 2012;93:1–15. doi:10.1016/j.epsr.2012.06.004.
[22] Barambones O, Alkorta P. Position Control of the Induction Motor Using an Adaptive Sliding-Mode Controller and Observers. IEEE Trans Ind Electron 2014;61:6556–65. doi:10.1109/TIE.2014.2316239.
[23] Rehman H, Derdiyok A, Guven MK, Longya Xu. A new current model flux observer for wide speed range sensorless control of an induction machine. IEEE Trans Power Electron 2002;17:1041–8. doi:10.1109/TPEL.2002.805579.
[24] Lascu C, Boldea I, Blaabjerg F. A Class of Speed-Sensorless Sliding-Mode Observers for High-Performance Induction Motor Drives. IEEE Trans Ind Electron 2009;56:3394–403. doi:10.1109/TIE.2009.2022518.
[25] Zorgani YA, Koubaa Y, Boussak M. MRAS state estimator for speed sensorless ISFOC induction motor drives with Luenberger load torque estimation. ISA Trans 2016;61:308–17. doi:10.1016/j.isatra.2015.12.015.
[26] Alsofyani IM, Idris NRN. A review on sensorless techniques for sustainable reliablity and efficient variable frequency drives of induction motors. Renew Sustain Energy Rev 2013;24:111–21. doi:10.1016/j.rser.2013.03.051.
[27] Tarchala G, Orlowska-Kowalska T. Equivalent-Signal-Based Sliding Mode Speed MRAS-Type Estimator for Induction Motor Drive Stable in the Regenerating Mode. IEEE Trans Ind Electron 2018;65:6936–47. doi:10.1109/TIE.2018.2795518.
[28] Schauder C. Adaptive speed identification for vector control of induction motors without rotational transducers. IEEE Trans Ind Appl 1992;28:1054–61. doi:10.1109/28.158829.
[29] Soltani J, Markadeh GRA, Abjadi NR, Ping HW. A new adaptive Direct Torque Control (DTC) scheme based-on SVM for adjustable speed sensorless induction motor drive. Proceeding Int. Conf. Electr. Mach. Syst. ICEMS 2007, 2007, p. 497–502. doi:10.1109/ICEMS.2007.4412013.
[30] Guezmil A, Berriri H, Pusca R, Sakly A, Romary R, Mimouni MF. Experimental Investigation of Passive Fault Tolerant Control for Induction Machine Using Sliding Mode Approach. Asian J Control 2018;21:520–32. doi:10.1002/asjc.1753.